

Self-Assembly and Orientation of Hydrogen-Bonded Oligothiophene Polymorphs at Liquid–Membrane–Liquid Interfaces

Ian D. Tevis,[†] Liam C. Palmer,[†] David J. Herman,[‡] Ian P. Murray,[‡] David A. Stone,[‡] and Samuel I. Stupp^{*,†,‡,§,⊥}

[†]Department of Chemistry, [‡]Department of Materials Science and Engineering, [§]Feinberg School of Medicine, and [⊥]Institute for Bionanotechnology in Medicine, Northwestern University, 2220 Campus Drive, Evanston, Illinois 60208, United States

S Supporting Information

ABSTRACT: One of the challenges in organic systems with semiconducting function is the achievement of molecular orientation over large scales. We report here on the use of self-assembly kinetics to control long-range orientation of a quarterthiophene derivative designed to combine intermolecular π – π stacking and hydrogen bonding among amide groups. Assembly of these molecules in the solution phase is prevented by the hydrogen-bond-accepting solvent tetrahydrofuran, whereas formation of H-aggregates is facilitated in toluene. Rapid evaporation of solvent in a solution of the quarterthiophene in a 2:1:1 mixture of 1,4-dioxane/tetrahydrofuran/toluene leads to self-assembly of kinetically trapped mats of bundled fibers. In great contrast, slow drying in a toluene atmosphere leads to the homogeneous nucleation and growth of ordered structures shaped as rhombohedra or hexagonal prisms depending on concentration. Furthermore, exceedingly slow delivery of toluene from a high molecular weight polymer solution into the system through a porous aluminum oxide membrane results in the growth of highly oriented hexagonal prisms perpendicular to the interface. The amide groups of the compound likely adsorb onto the polar aluminum oxide surface and direct the self-assembly pathway toward heterogeneous nucleation and growth to form hexagonal prisms. We propose that the oriented prismatic polymorph results from the synergy of surface interactions rooted in hydrogen bonding on the solid membrane and the slow kinetics of self-assembly. These observations demonstrate how self-assembly conditions can be used to guide the supramolecular energy landscape to generate vastly different structures. These fundamental principles allowed us to grow oriented prismatic assemblies on transparent indium-doped tin oxide electrodes, which are of interest in organic electronics.



INTRODUCTION

Highly organized molecules with tailored morphologies across scales are of great importance to future technologies, such as thin-film organic electronic devices.¹ In order to obtain a semiconducting organic material with properties necessary for efficient devices there must be spatial overlap of π -orbitals among adjacent conjugated molecules. This overlap generates large bandwidths for valence or conduction bands to assist charge hopping among molecules by shortening intermolecular distances.^{2–9} Reducing grain boundaries or lattice defects can increase charge mobilities of crystalline organic semiconductors by lowering the number of carrier traps.¹⁰ Research on crystalline organic semiconductors has also revealed anisotropic carrier mobilities along crystallographic axes that have different degrees of π -orbital overlap, thus demonstrating the influence that molecular packing, orientation, and morphology can have on electronic properties.^{2–9,11,12} Designing solution-processable organic semiconductors requires innovative approaches to control ordering and allow efficient charge transport while minimizing the defects that typically arise from solution casting.^{2,6} Conjugated molecules tend to have poor solubilities because strong π – π interactions drive crystalline domain formation,

leading to precipitation. Introducing solubilizing groups can frustrate packing, causing disordered film morphologies after deposition from solution. The organization of such molecules can be controlled by rationally designing their covalent structure to assemble in a specific way and also by controlling environmental factors during deposition.

In order to offset the disorder caused by solubilizing groups, supramolecular interactions, such as hydrogen bonding, can be used to bring conjugated molecules in close proximity to promote large spatial π -orbital overlap while maintaining their solution processability. Numerous π -conjugated molecules have been found to spontaneously self-assemble in solution into a variety of one-dimensional (1D) nanostructures by modifying the chemical structure and varying external factors, like solvent, temperature, and substrate to form nanofibers, nanotubes, or nanorods with uniform morphological dimensions.^{12–28} Self-assembling organic molecules have been synthesized by our group in a variety of architectures, utilizing conjugated molecules, like oligothiophenes and oligo(*p*-phenylene vinylene),

Received: May 25, 2011

Published: August 31, 2011

as semiconductor units to form semiconducting 1D nanostructures.^{12,20,22,29–31} Oligothiophene derivatives consist of thiophene units connected by α -linkages with solubilizing groups attached at the terminal α -positions imparting the molecule with a high degree of π -orbital overlap and solubility.^{11,32} Oligothiophene has a low band gap³³ and can be easily derivatized into many covalent architectures, and the solution and solid-state aggregation of oligothiophenes has been well characterized for use in opto-electronic devices.^{34,35} Oligothiophenes have also been proven to be viable electronic materials for efficient photovoltaic devices.^{36,37}

Control over morphology has been recently studied in the n-type semiconductor C₆₀ and its derivatives by amphiphilic assembly, templated synthesis, and crystallization/precipitation. Diverse structures ranging from nanowhiskers, nanofibers, spheres, and flower-like nanoscale objects as well as hexagonal, rhombohedral, and mixed polygonal sheets have been obtained.^{38–50} A common crystallization/precipitation technique used to create polymorphs at solvent interfaces has been termed liquid–liquid interfacial precipitation (LLIP).⁴² In a typical LLIP experiment, C₆₀ is dissolved into a “good” solvent, such as toluene, and then a “poor” solvent, such as isopropanol, is gently poured on top to form a liquid–liquid interface. Over time, the “poor” solvent slowly diffuses into the “good” solvent, decreasing the solubility of C₆₀ to the point of supersaturation and nucleation of structures. Following nucleation, myriad structures are obtained depending on solvent, temperature, and chemical structure of the C₆₀ derivative. Assembly at solvent interfaces has great potential to produce unique structures and also to spontaneously organize molecules into ordered materials.^{51–53} Specifically, we recently found a solid diffusion barrier formed by self-assembly to separate two liquids that yields a hierarchically ordered membrane.⁵¹

Inspired by our interfacial assembly studies, the known polymorphism of C₆₀, and examples of supramolecular interactions in highly organized molecules,^{54–57} we explore here self-assembly pathways of a new small conjugated molecule and the utilization of a porous solid membrane as a diffusion barrier between two solutions. Only one solution contained the conjugated molecule, but each differed in the amount of the “poor” solvent that promotes self-assembling behavior. Scanning electron microscopy (SEM) and grazing incidence small-angle X-ray scattering (GISAXS) were used as tools to identify morphology, internal organization, and orientation of the resulting structures. The new molecule used in this study (structure shown in Figure 1) has the ability to aggregate through both hydrogen bonding and π – π stacking, and it is very similar to a semiconducting molecule reported recently by us and others.^{24,58} Molecules that combine both of these interactions have been known to self-assemble into 1D aggregates and form gels as a result of network formation at low concentrations.^{12,59–61}

RESULTS AND DISCUSSION

Oligothiophene Self-Assembly. We synthesized the soluble self-assembling quarterthiophene molecule, termed here **4TG-EH**, shown in Figure 1, using previously reported synthetic methodologies.⁵⁸ A detailed description of the molecular synthesis and characterization can be found in the Supporting Information (Figure S1). Assembly of the quarterthiophene core is assisted by hydrogen bonding among the four amide groups surrounding the core. The self-assembling quarterthiophene moiety is converted to a soluble compound by attaching gallic acid groups at each terminus with six branched 2-ethylhexyl groups in total. These groups should somewhat frustrate packing



Figure 1. Molecular structure of a self-assembling oligothiophene derivative. Quarterthiophene core shown in red and hydrogen-bonding groups in blue. Solubility is enhanced by substitution of the core by 3,4,5-tris(2'-ethylhexyl)benzoate (shown in green).

of molecules relative to molecules with straight alkyl chains.⁶² A molecule similar to **4TG-EH** with unbranched alkyl solubilizing groups was previously found to dissolve in solvents, such as tetrahydrofuran (THF), that have an affinity for alkyl and conjugated moieties and can also accept hydrogen bonds to compete with that molecule's self-assembly.⁵⁸ In solvents like toluene, that same molecule was reported to form solvated H-aggregates.⁵⁸ A concentration study of **4TG-EH** in both THF and toluene was performed and monitored by UV–vis spectroscopy in order to probe the aggregation properties of the molecule. In THF solutions, the absorbance λ_{max} appeared at approximately 415 nm for all concentrations measured between 10^{-5} and 10^{-3} M (Figure S2 and Table S1, Supporting Information). In great contrast, the toluene solutions exhibited a 21 nm blue shift in λ_{max} from 416 to 395 nm as the concentration increased (Figure S2 and Table S2, Supporting Information). A decrease in fluorescence intensity and 6 nm red shift was observed when switching from THF to toluene (Figure S2, Supporting Information). The blue shift in absorption, red shift in fluorescence, and fluorescence decrease all indicate that the aromatic oligothiophene core is forming a face-to-face H-aggregate.⁶³ These markers of solution-phase H-aggregation of **4TG-EH** are less intense than our previously reported molecule with unbranched alkyl chains; in that system, a 42 nm blue shift in UV–vis absorbance, a 51 nm red shift in fluorescence, and significant fluorescence quenching were observed.⁵⁸ We attribute these differences to the packing frustration provided by the branched alkyl solubilizing groups. We conclude from these spectroscopic observations that self-assembly of this molecule is inhibited by “good” solvents, such as THF, and the formation of H-aggregates can be promoted in a “poor” solvent, like toluene.

Liquid–Vapor Precipitation. Molecular packing frustration in **4TG-EH** as a result of the six branched alkyl groups was expected to play a significant role during drying in the self-assembly of this molecule under kinetic versus thermodynamic control. The solvent THF has a high vapor pressure and evaporates rapidly, which may kinetically trap the **4TG-EH** during drying in a morphology with poor π -orbital overlap. Addition of 1,4-dioxane, which is also a good solvent but has a lower vapor pressure, should slow evaporation and allow molecules to access kinetically more stable supramolecular structures. We blended dioxane and THF in a 2:1 ratio to create a “good” solvent that could dissolve **4TG-EH**. Blending this “good” solvent mixture with a “poor” solvent, such as toluene, gave us a solution that dissolves **4TG-EH**, evaporates slowly, and can promote self-assembly by addition of more toluene. The work described here utilized a blend of 2:1:1 dioxane/THF/toluene to dissolve **4TG-EH** into 2.5 wt % solutions. Solutions were heated in order to dissolve and disaggregate molecules and were then allowed to cool to room temperature before use. We drop cast 10 μL of the **4TG-EH** solution onto a clean

poly(tetrafluoroethylene) (PTFE) sheet. The drop remained stationary at the location of drop casting and was allowed to dry in a covered Petri dish (Figure 2). The resulting dried film was sputter coated with 10 nm of Au/Pd and imaged by SEM. In the micrographs, 1D structures can be observed as a mat of fibers covering the surface of the PTFE (Figure 3a and d). The observed structures can be tens of micrometers long and range in diameter from hundreds to thousands of nanometers with the long axis of the bundles parallel to the substrate. The length of the 4TG-EH was estimated by molecular modeling to be 5.9 nm in its extended conformation. This length is significantly smaller than the observed diameters in the SEM, indicating the occurrence of a high extent of bundling. We expect that the 4TG-EH does not adhere to the fluorinated substrate because of PTFE's low surface energy. This implies that the fibrous assembly of molecules occurs in solution, precipitates, and then grows as the solution dried. These fibrous structures are common for self-assembling molecules similar to 4TG-EH, and we assume that the π - π stacking direction is parallel to the long axis of the bundled fibers.¹⁵

Slow Drying. The interplay between intermolecular forces used to direct self-assembly and the solvent environment can have dramatic effects on nanoscale organization.^{64–67} We therefore repeated the fibrous growing conditions with a slight change

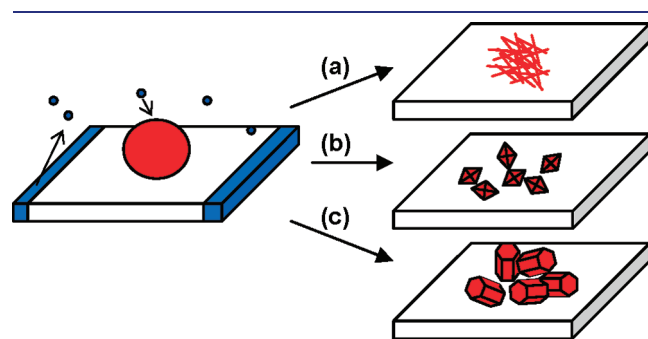


Figure 2. Selective formation of various polymorphs from solvated 4TG-EH (red) on a sheet of PTFE (white). (a) 2.5 wt % 4TG-EH without toluene vapor (blue). (b) 2.5 wt % 4TG-EH with toluene vapor. (c) 5 wt % 4TG-EH with toluene vapor.

to the sample environment. We drop cast 10 μ L of the same 2.5 wt % solution of 4TG-EH onto a piece of clean PTFE and allowed it to dry in covered Petri dish with a toluene-saturated atmosphere (see Figure 2b). Over time toluene vapors diffused into the droplet and lowered the solubility of the 4TG-EH, and after several hours, the droplet dried. We observed by SEM that slow drying of the solvent results in the growth of faceted and regular structures instead of only fibers. The structures had rhombohedral shapes and ranged in size from 1 μ m to a little over 10 μ m across (see Figure 3b). As revealed in Figure 3b, we also observed bundles of fibers in addition to the rhombohedra. The rhombohedra typically have one axis longer than the other, and high-magnification images of their surfaces reveal striations perpendicular to the short axis of the rhombohedra. We hypothesize that the π - π stacking direction coincides with these observed striations.¹⁵ Rhombohedra were also observed to precipitate from solutions of 4TG-EH aged overnight in a sealed vessel. In fact this solution-aging method proved to be a more reproducible pathway to obtain larger rhombohedra with a minimum amount of fibers (Figure 3e).

SEM micrographs of the rhombohedra suggest a possible growth mechanism. We observed fibers growing from the rhombohedra along the direction of the striations (see Figure 3e). We believe these fibers are the first structures formed through a fast process, and toluene is likely to become a part of the structure around the rapidly formed fibers. The presence of solvent in initially nucleated self-assembled structures has been proposed previously by the Meijer group.⁶⁸ Ostwald's rule of order states that the least stable polymorph forms first and then gets converted to a more stable polymorph.^{65,69} After the initial nucleus forms, additional adhering molecules should allow it to grow, but the initial growth is metastable. The fibers formed are a metastable state that slowly convert to the more stable rhombohedra, which remain when drying is complete. This argument is supported by the previously observed fibers that formed from faster drying droplets. Another possible mechanism for the formation of rhombohedra starts with initial formation of fibers that further grow into rhombohedra from dissolved molecules. Both mechanisms are possible and most likely both occur to some extent. In micrographs containing both bundled fibers and rhombohedra (see Figure 3b), the two structures are never

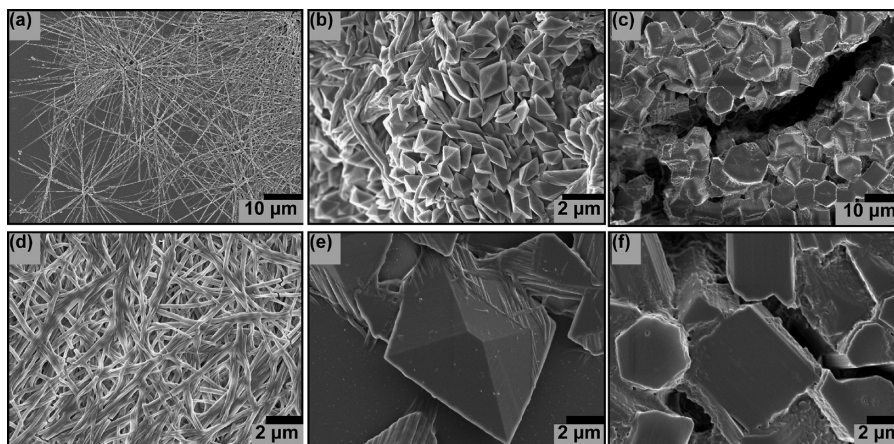


Figure 3. SEM micrographs of polymorphs formed under different conditions on PTFE. (a and d) Bundled fibers formed from a 2.5 wt % solution without toluene vapor. (b) Rhombohedra interspersed with bundled fibers formed from a 2.5 wt % solution with toluene vapor. (c and f) Randomly oriented hexagonal prisms formed from a 5 wt % solution with toluene vapor. (e) Larger rhombohedra precipitated from an aged 2.5 wt % solution with fibers growing along the striations of the rhombohedra.

observed to be directly connected, which implies that the nucleation and growth of rhombohedra occur separately from bundled fiber formation.

Effect of Higher Concentration. Higher concentrations may also affect morphology by increasing the likelihood of rapid nucleation and growth. This faster nucleation and growth is likely to favor the metastable state, and in the case of 4TG-EH, we assumed it would be the fiber morphology. At high enough concentrations in the “poor” solvent (toluene), molecules similar to 4TG-EH have been shown to gel by forming interpenetrating networks of fibers.^{24,58} In our experimental solvent blend, gel formation is not observed even at concentrations as high as 5 wt % after aging for 30 days. The same precipitation observed in 2.5 wt % solutions was not observed in 5 wt % solutions. This implies that in aged solutions at the 5 wt % concentration, self-assembly occurs quickly and traps the 4TG-EH into the metastable fiber morphology without conversion to a more stable polymorph over time. We drop cast 10 μL of a heated then cooled solution of 5 wt % 4TG-EH onto a clean flat piece of PTFE in a Petri dish containing an atmosphere saturated with toluene. This droplet dried slowly over several hours, resulting in a film. SEM of this film reveals a third morphology consisting of hexagonal prisms ranging in size from 3 to 10 μm across and about 1 to 5 μm in height (Figure 3c and f). Almost all of the 4TG-EH converted to hexagonal prisms in these samples with fibers appearing at the periphery of the dried droplet where drying occurred first and also covering some of the hexagonal structures. As revealed in the micrograph of Figure 3f, we observe several rectangular objects that are actually hexagonal prisms on their sides. This side view of the prisms, as well as the fractured prism in the lower right portion of Figure 3f, demonstrates clearly the presence of striations along the long axis of the prism. Based upon our observations, the rhombohedra appear to be the thermodynamic product, and the hexagonal prisms and fibers are kinetically trapped structures. The propensity of 4TG-EH to form a regular structure like a rhombohedra coupled with its conformational flexibility may force it to adopt other structures like hexagonal prisms when conditions favor a kinetically trapped structure.

Structural Characterization. The internal organization of these dried polymorphs was characterized by UV–vis spectroscopy and Fourier transform infrared spectroscopy (FTIR). The normalized transmission UV–vis data (Figure S3, Supporting Information) demonstrate that all three dried polymorphs have different λ_{max} positions. The rhombohedra have a λ_{max} closer to the solution-phase unassembled molecule at 411 nm. The dried fibers have a λ_{max} of 402 nm, which is between the solution-phase assembled and nonassembled states. On the other hand, the hexagonal pillars have a maximum absorbance at 386 nm, which is close to the absorbance we attributed to the H-aggregated solution assembly of 4TG-EH, which was 395 nm. The internal organization of the quarterthiophene core in the rhombohedra and fibers is probably not the same aggregated structure that occurs in the hexagonal prisms and solvated assemblies. In order to further probe the internal organization of these polymorphs, powders of all three polymorphs were prepared on PTFE sheets and transferred to a ZnSe crystal for FTIR analysis. Transmission FTIR presented in Figure S4, Supporting Information, shows the similarities of the vibrational profile of all three polymorphs. We observed a shift of the N–H stretch from 3312 to 3314 to 3320 cm^{-1} from rhombohedra, to fibers, to hexagons, respectively. The position of this N–H stretch observed at about 3300 cm^{-1} is indicative of an amide involved in hydrogen

bonding, as expected for a solid cast from low-polarity solvents. We suspect this hydrogen bonding is intermolecular, since intramolecular hydrogen bonding would involve formation of a seven membered ring that would need to be strong enough to compete with intermolecular hydrogen bonding at the high concentrations as the solvent evaporates. The lower energy transitions in the region around 800 cm^{-1} show vibrations characteristic of ordered oligothiophenes.⁷⁰ Amorphous oligothiophenes, such as solvated molecules, should show only a single peak in this region that can be attributed to one γ -CH-out-of-plane vibration. This peak would then split as the oligothiophenes aggregate.⁷⁰ There are minor differences in the position of the peaks, but the general shape is the same for all three polymorphs, which shows that the oligothiophene core is not amorphous. This result is significant since the UV–vis spectra show that rhombohedra have a λ_{max} similar to the solvated molecule, hexagonal prisms with a λ_{max} similar to the aggregated molecules, and the fibers somewhere in between. Therefore, it appears that the quarterthiophene units in the three different morphologies are aggregated but possibly at different angles, giving slightly different peak positions observed in the FTIR and different λ_{max} in the UV–vis.

The three polymorphs are easily accessible by this simple liquid–vapor technique, but orientation of the polymorphs is not well-defined. The bundled fibers mostly lie in a 2D mat with their long axis parallel to the substrate; rhombohedra lie flat on the surface with striations also parallel to the substrate; and the hexagonal prisms are randomly oriented with respect to the substrate. Facilitating charge mobility through long-range molecular orientation with respect to electrodes is of course functionally important in devices, such as field-effect transistors and solar cells. For example, in photovoltaic devices the ideal orientation of conducting pathways is perpendicular to electrode planes.⁷¹ We demonstrate below how a self-assembly pathway was found in the system investigated here utilizing a liquid–membrane–liquid interface.

Liquid–Membrane–Liquid Interfacial Precipitation. Recent examples from our laboratory of hierarchically ordered structures formed at liquid–liquid interfaces⁵¹ and from the literature of vertically aligned C₆₀ microtubes by liquid–membrane–liquid interfacial precipitation⁵² inspired us to develop a different pathway for the self-assembly of the molecule investigated here. A 5 wt % solution of 4TG-EH in a 1:1 blend of THF/toluene was gently poured onto a solution of toluene forming a liquid–liquid interface, and the vial was sealed to prevent evaporation. Over time the toluene diffused into the 4TG-EH, promoting it to assemble. The resulting structure consisted solely of fibers with no other polymorphs present. From our liquid–liquid interfacial experiments described above, it is clear that diffusion occurs quickly between these solutions, favoring metastable fiber formation. We hypothesized that introducing a porous barrier between the two liquids could further slow diffusion of the solvent that promotes self-assembly and allow the selective formation of polymorphs and potentially the creation of new polymorphs. Anodic aluminum oxide (AAO) membranes with straight transmembrane cylindrical channels of 200 nm diameters were used as a diffusion barrier between the 4TG-EH solution and the toluene solvent. We placed toluene on one side of a vertically oriented AAO membrane and then a solution of 5 wt % 4TG-EH on the other (Figure 4). Over time the two solutions diffused into each other to create a region of increased toluene concentration at the liquid–membrane–liquid interface,

and over time the solutions dried. Again, only fibers were observed, and we concluded the AAO membrane alone was not sufficiently slowing down toluene diffusion. We considered that diffusion across the interface of two liquids can also be controlled by increasing their viscosities and thus chose to control the viscosity of our toluene solution by dissolving a high concentration (20 wt %) of a high molecular weight poly(methyl methacrylate) (PMMA) (M_n : 996 000 Da). The high-viscosity solution was used in addition to the vertically supported AAO membrane to slow diffusion of toluene into the solution of 4TG-EH, producing a region of increased toluene concentration at the liquid–membrane–liquid interface (see Figure 4). A detailed description and diagram of the mounted membrane setup can be found in the Supporting Information (Figure S5). We placed the viscous toluene solution on one side of a mounted AAO membrane and observed it to wet the membrane making it translucent, but it did not flow to the other side. On the other side of membrane, we placed 10 μL of a 2.5 wt % 4TG-EH solution in 2:1:1 dioxane/THF/toluene and allowed it to dry over hours. The AAO membrane was held vertically, causing the solution

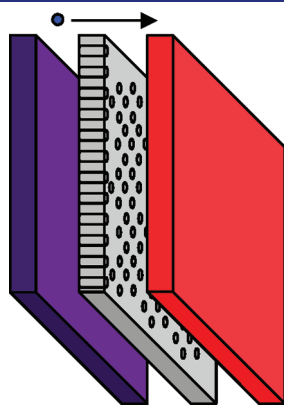


Figure 4. Schematic of liquid–membrane–liquid deposition setup using an AAO membrane to slow the diffusion of solvent between two solutions. The compartment to the left of the membrane contains a viscous toluene solution of PMMA shown in purple. Toluene, shown in blue, traverses the membrane into the right compartment containing a 4TG-EH solution, shown in red, creating a region of higher toluene concentration at the interface.

to dry and concentrate downward toward the bottom of the AAO. The resulting structures are rhombohedral with lengths of the long axis of about 2 μm (Figure 5a and d). The rhombohedra are the dominant morphology in this case, appearing as large aggregates near the bottom of the dried sample. Increasing the concentration to 5 wt % 4TG-EH produces the same hexagonal structure observed using the original liquid–vapor method on PTFE but with one major difference. We found that the hexagonal prisms are all anchored to the surface of the AAO and growing perpendicular to the surface (Figure 5b and e) forming oriented pillars. There are visible striations in the SEM micrograph of the pillars (see Figure 5e) that run along a direction perpendicular to the substrate. From these experiments it is unclear if the directionality of toluene diffusion through the membrane (see Figure 4) induces the observed oriented growth of hexagonal pillars on the surface of the membrane. These hexagonal pillars cover the entire surface of the AAO in contrast to the rhombohedra, which are found mostly at the bottom of the dried membrane. Concentration has the same effect on morphology as the liquid–vapor technique, but the AAO substrate and directionality of solvent flow affords control over long-range orientation of the hexagonal prisms.

A hexagonal pillar grown on an AAO membrane was thinned with a focused ion beam and attached to a probe for imaging by transmission electron microscopy (TEM) (Figure 6). In Figure 6b the thinned AAO membrane is visible as the darker pore structure on the bottom, and the 4TG-EH is the solid gray material on the top. There are visible regular striations in the 4TG-EH pillar running perpendicular to the surface of the AAO pores and to some extent into the pores. Fast Fourier transform (FFT) of a section of the TEM micrograph shows that the striations are indeed regular. Image profiles and the FFT spacing indicate a spacing of 5.55 nm which indeed corresponds to the length of the conjugated molecule, which is ~ 5.9 nm as determined by molecular modeling. These TEM micrographs suggest that the long axis of the molecule lies parallel to the surface plane of the AAO, and the π – π stacking direction is perpendicular to the substrate along the direction of the observed striations.

Role of Surface Polarity. Modifying the solvent viscosity and introducing a porous diffusion barrier have proven to be useful techniques for controlling the aggregation and orientation of this

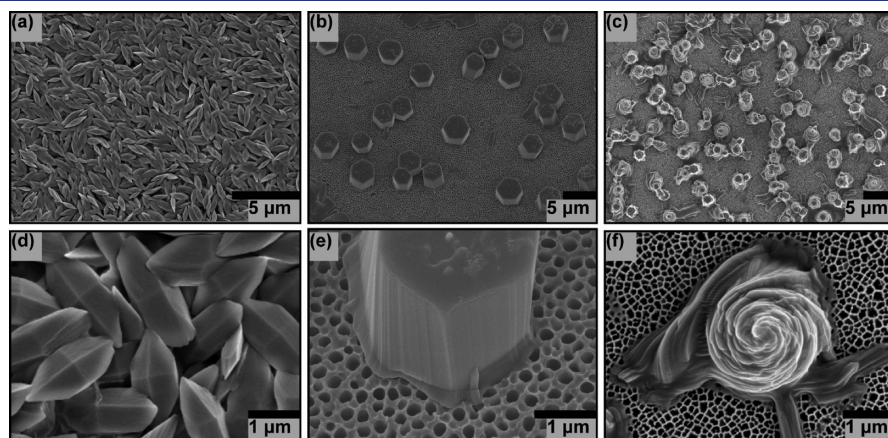


Figure 5. SEM micrographs of polymorphs formed on an AAO membrane. (a and d) Rhombohedra precipitated from a 2.5 wt % solution. (b) Anchored hexagonal prisms growing perpendicular to substrate from a 5 wt % solution. (c and f) Bundled fibers formed from a 5 wt % solution at 0 °C attached and growing perpendicular to the substrate. (e) Higher magnification micrograph of hexagonal prisms showing striations along the long axis of the prisms perpendicular to the substrate.

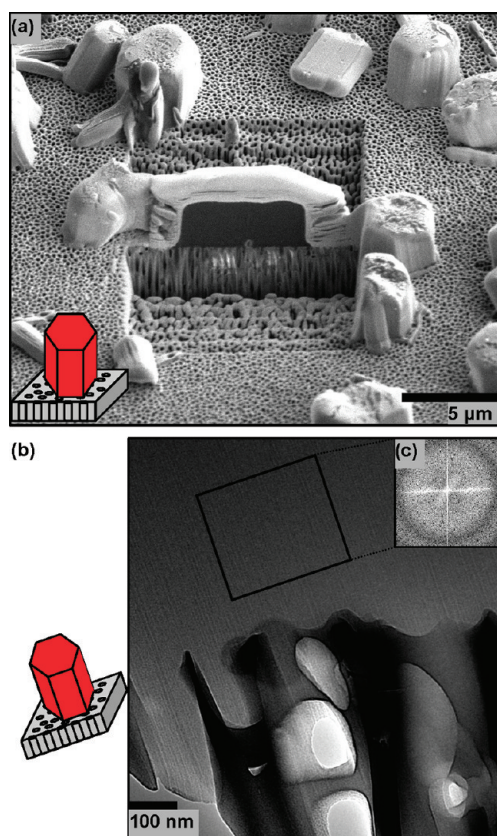


Figure 6. Micrographs illuminating internal structure of hexagonal prisms grown on an AAO membrane with cartoons included for clarity. (a) SEM micrograph of hexagonal prism coated by a line of platinum and thinned by a focused ion beam. (b) TEM micrograph of a thinned prism and the underlying porous membrane. Cross-section of pores is visible on the bottom of the image, while the thinned 4TG-EH structure can be seen on the top of the image. (c) FFT of section of TEM micrograph indicating regularity of striations.

hydrogen-bonded conjugated oligomer and could provide additional tools to probe the aggregation of these molecules. One particularly interesting tool is surface polarity modification.⁷² It is evident by comparing the hexagonal pillars and rhombohedra that the AAO surface plays a significant role in their nucleation and growth. Rhombohedra were not observed directly growing from the AAO membrane, and this implies that they form through a homogeneous nucleation pathway. Hexagonal prisms were observed by SEM to grow either through a homogeneous nucleation pathway during the previously described experiment on a PTFE sheet (see Figure 3c and f) or from a heterogeneous nucleation pathway on an AAO membrane (see Figure 5b and e). Therefore the surface energy of the substrate was expected to have a strong impact on the nature of the 4TG-EH structure nucleated. The amide groups are likely to interact and adsorb onto the polar aluminum oxide surface, so increasing the polarity of this surface was expected to increase its affinity for the amide groups and thus direct the self-assembly pathway toward heterogeneous nucleation (we accomplished this surface modification with a 10 min UV-ozone treatment of the AAO). A 2.5 wt % solution of 4TG-EH known to form rhombohedra was used to test the effect that surface modification has on their growth. By changing this parameter, we observed a transition from exclusively rhombohedra to exclusively hexagonal prisms (Figure S7,

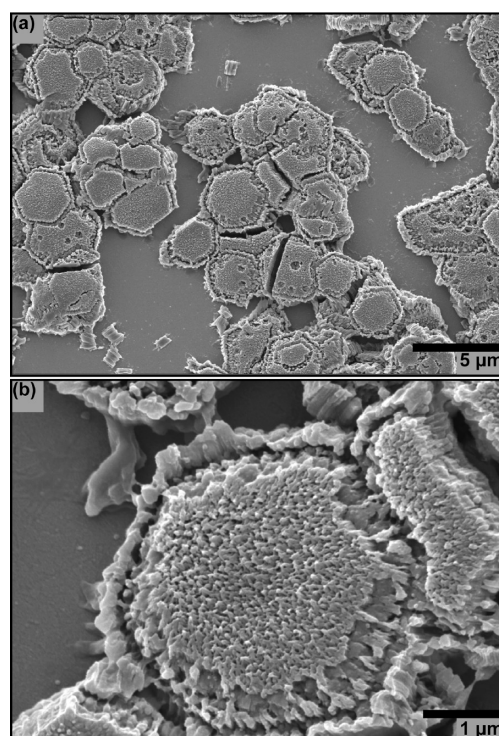


Figure 7. SEM micrographs of hexagonal prism grown on ITO. (a) Low-magnification image of several hexagonal pillars. (b) High-magnification image of hexagonal pillar demonstrating fibrous growth on the external surfaces of the prism.

Supporting Information), even at this lower concentration. We speculate that increasing the surface polarity allows more 4TG-EH molecules to adsorb to the surface, which coupled with the higher concentration of toluene at the liquid–membrane–liquid interface increases the likelihood that adsorbed molecules would favor heterogeneous nucleation of the hexagonal pillars. As mentioned above, we believe the hexagonal pillars grow from a nucleus perpendicular to the plane of the membrane by a heterogeneous nucleation and growth pathway.

Role of Temperature. Lower temperatures should favor the metastable structure, since molecules have less energy to move and rearrange into a more stable state. Solvent evaporation is slower at lower temperatures, which allowed us to use the binary solvent system of 1:1 THF/toluene instead of the more complex ternary system used previously. A 5 wt % solution of 4TG-EH was placed in the vertical setup shown in Figure 4 with UV-ozone treated AAO membrane and allowed to dry slowly at 0 °C. We observed twisted bundled fibers growing perpendicular to the AAO membrane (Figure 5c and f). The UV-ozone treated AAO membranes allow more 4TG-EH molecules to adsorb to the surface ultimately leading to nucleation. The initial structure formed in this case is the metastable fibrous polymorph, but at these lower temperatures, the metastable phase cannot convert to the more stable hexagonal polymorph. As the solution dries, the fibrous growth continues perpendicular to the substrate in a manner similar to hexagonal prisms, but the entire structure remains trapped as bundled fibers.

Deposition onto a Nonporous ITO Electrode. From the experiments described above, it is clear that polymorph directing factors, like concentration, temperature, and substrate polarity, can control the structure of this hydrogen-bonded conjugated

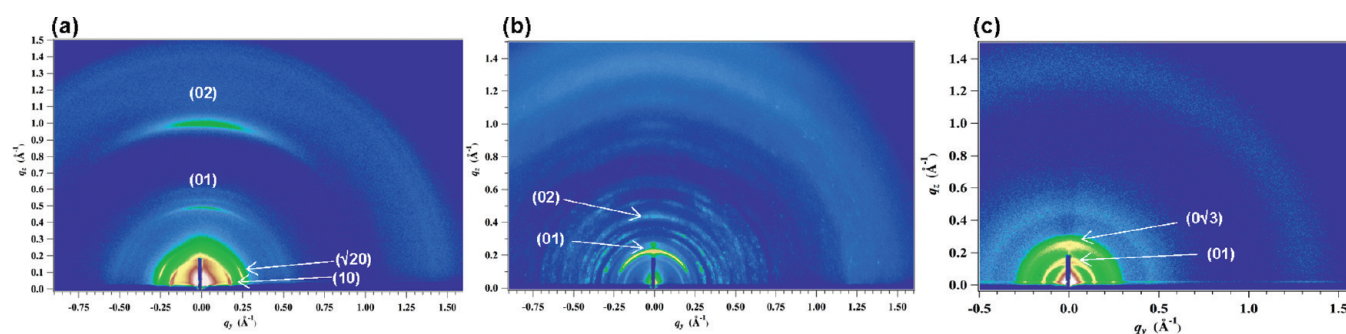


Figure 8. 2D-GISAXS patterns of (a) perpendicularly oriented hexagonal pillars, (b) randomly oriented rhombohedra microcrystals, and (c) mats of bundled fibers deposited onto ITO substrates.

oligomer. It is not clear, however, to what extent the porous nature of the substrate surface and the delivery method of a “poor” solvent affects the polymorphism of this molecule. The porous membrane made from AAO is an opaque insulator and is not immediately applicable to optoelectronic devices. Therefore, we were also interested in self-assembly behavior on a solid metal-oxide film, such as indium tin oxide (ITO), which is highly transparent and highly conductive but not porous. Using the observations made possible from the liquid–membrane–liquid technique that the hexagonal polymorph can be selected over the others by increasing the 4TG-EH concentration, slowly delivering toluene, and depositing onto a hydrophilic UV-ozone treated surface, we attempted to grow hexagonal prisms directly onto an ITO electrode. A 10 μL drop of 5 wt % 4TG-EH in 1:1 THF/toluene was drop cast and spread across a UV-ozone treated ITO electrode and was placed in a Petri dish with a toluene-saturated atmosphere. After drying, the resulting microstructure is the hexagonal polymorph growing perpendicular to the ITO substrate (Figure 7). If growth of these structures is allowed to continue, eventually they coalesce to form sheets (Figure S8, Supporting Information). These results show that the directionality of solvent flow present in liquid–membrane–liquid interfacial precipitation (see Figure 4) is not necessary to induce the observed oriented growth (see Figures 5e and 7). The source of orientation in this polymorph appears to originate from interactions of the molecules with the metal-oxide surface. Based on SEM observations, the growth of pillars might proceed through the metastable fibrous structures as observed in rhombohedra (Figure 7b). The drying process trapped the metastable states on the external surfaces of the hexagonal prisms, which stay attached to the top surface but separated from the sides of the prisms upon drying. We propose that the external surfaces of the hexagonal prisms grow by first forming a metastable fibrous state that then slowly rearranges and converts to the hexagonal structure. We did not observe these fibrous structures in the case of growth on an AAO membrane most likely because the solutions cast on ITO dried at a faster rate.

Two-dimensional GISAXS (2D-GISAXS) is a powerful technique for determining internal structure and orientation of self-assembled structures relative to a substrate.⁷² 2D-GISAXS data were obtained for the hexagonal pillars grown on ITO, films of rhombohedra deposited on ITO, and mats of fibers deposited on ITO (see Figure 8). The hexagonal pillars (Figure 8a) demonstrated a preferred orientation of molecules with respect to the substrate surface, as evidenced by the anisotropic scattering intensity in the 2D-GISAXS data. The (10) and ($\sqrt{20}$) peaks along the equatorial direction correspond to a cubic packing

arrangement of molecules in the x – y plane, with a d -spacing of 32.9 Å. This distance corresponds roughly to the length of the rigid aromatic core of the molecule plus the hydrogen-bonding amide groups (34 Å), indicating that the long axis of the molecule runs parallel to the ITO substrate in the x – y plane. The (01) and (02) peaks correspond to a d -spacing of 11.9 Å perpendicular to the substrate surface in the z -direction. This d -spacing does not match to any obvious intermolecular distance and is likely due to a tilted arrangement of molecules within the pillar structure. Comparing the anisotropic 2D-GISAXS pattern with our TEM and SEM results, we expect that the z -direction is also the direction of π – π stacking. The rhombohedra (Figure 8b) show several spots indicating that the internal structure of the polymorph is highly ordered. The (01) and (02) peaks correspond to a d -spacing of 24.4 Å. The other bright spots indicate order along various crystallographic axes, but the polycrystallinity of this sample too complex for complete analysis. We were unable to grow crystals of sufficient size for single-crystal analysis. The fibers (Figure 8c) demonstrate less orientation than the hexagonal pillars with the (01) peak corresponding to 41.0 Å and the (0 $\sqrt{3}$) peak indicating weak hexagonal packing. In summary, all three polymorphs have significantly different internal structures. For electronic applications, the hexagonal pillars (Figure 8a) may have an optimal structure, with molecular stacking perpendicular to the substrate surface and H-aggregated π – π stacking between molecules. For photovoltaic devices, these interactions would provide high-mobility pathways through π – π stacked structures and short distances for carriers to travel to electrodes.

CONCLUSIONS

We have shown strong polymorphism and control of molecular orientation in the self-assembly of a semiconducting conjugated molecule with capacity to form hydrogen bonds. Selection of a self-assembly pathway that involves nucleation on a surface and exceedingly slow aggregation of molecules was found to result in highly oriented prismatic structures that could be of interest for electronic function. These observations demonstrate how the supramolecular energy landscape can be guided by external conditions to modify the structural nature of assemblies formed by conjugated organic molecules.

ASSOCIATED CONTENT

S Supporting Information. Complete synthetic details of 4TG-EH, UV–vis, fluorescence and FTIR spectra, detailed

growth setup of polymorphs on AAO membrane, SEM micrographs of hexagonal structures grown under different conditions, TEM micrographs of hexagonal structure, SEM of hexagonal structures grown on ITO, and complete citation for ref 47. This material is available free of charge via the Internet at <http://pubs.acs.org>.

AUTHOR INFORMATION

Corresponding Author

s-stupp@northwestern.edu

ACKNOWLEDGMENT

This work was supported by the U.S. Department of Energy Office of Science, Office of Basic Energy Sciences (DE-FG02-00ER45810) as well as support for L.C.P. from the National Science Foundation (DMR-0605427). X-ray measurement diffraction experiments were carried out at beamline 8-ID-E of the Advanced Photon Source at Argonne National Laboratory. Use of the Advanced Photon Source at Argonne National Laboratory was supported by the U.S. Department of Energy, Office of Science, Office of Basic Energy Sciences, under contract no. DE-AC02-06CH11357. This work also made use of the Electron Probe Instrumentation Center (EPIC) for SEM, TEM, and SEM/FIB, the Keck Biophysics Facility for the UV-vis and fluorescence spectroscopy, Keck II for FTIR spectroscopy, and IMSERC for NMR and mass spectrometry. We thank B. Meyers for his assistance with TEM sample preparation, H. C. Fry for his synthetic assistance, and J. W. Strzalka for his assistance and X-ray expertise.

REFERENCES

- (1) Hirst, A. R.; Escuder, B.; Miravet, J. F.; Smith, D. K. *Angew. Chem., Int. Ed.* **2008**, *47*, 8002–8018.
- (2) Sundar, V. C.; Zaumseil, J.; Podzorov, V.; Menard, E.; Willett, R. L.; Someya, T.; Gershenson, M. E.; Rogers, J. A. *Science* **2004**, *303*, 1644–1646.
- (3) Podzorov, V.; Menard, E.; Borissov, A.; Kiryukhin, V.; Rogers, J. A.; Gershenson, M. E. *Phys. Rev. Lett.* **2004**, *93*, 086602.
- (4) Zeis, R.; Besnard, C.; Siegrist, T.; Schlockermann, C.; Chi, X. L.; Kloc, C. *Chem. Mater.* **2006**, *18*, 244–248.
- (5) Lee, J. Y.; Roth, S.; Park, Y. W. *Appl. Phys. Lett.* **2006**, *88*, 252106.
- (6) Sirringhaus, H.; Brown, P. J.; Friend, R. H.; Nielsen, M. M.; Bechgaard, K.; Langeveld-Voss, B. M. W.; Spiering, A. J. H.; Janssen, R. A. J.; Meijer, E. W.; Herwig, P.; de Leeuw, D. M. *Nature* **1999**, *401*, 685–688.
- (7) Moon, H.; Zeis, R.; Borkent, E. J.; Besnard, C.; Lovinger, A. J.; Siegrist, T.; Kloc, C.; Bao, Z. N. *J. Am. Chem. Soc.* **2004**, *126*, 15322–15323.
- (8) Mas-Torrent, M.; Hadley, P.; Bromley, S. T.; Ribas, X.; Tarres, J.; Mas, M.; Molins, E.; Veciana, J.; Rovira, C. *J. Am. Chem. Soc.* **2004**, *126*, 8546–8553.
- (9) Lan, Y. K.; Huang, C. I. *J. Phys. Chem. B* **2009**, *113*, 14555–14564.
- (10) Coropceanu, V.; Cornil, J.; da Silva, D. A.; Olivier, Y.; Silbey, R.; Bredas, J. L. *Chem. Rev.* **2007**, *107*, 926–952.
- (11) Garnier, F.; Yassar, A.; Hajlaoui, R.; Horowitz, G.; Deloffre, F.; Servet, B.; Ries, S.; Alnot, P. *J. Am. Chem. Soc.* **1993**, *115*, 8716–8721.
- (12) Messmore, B. W.; Hulvat, J. F.; Sone, E. D.; Stupp, S. I. *J. Am. Chem. Soc.* **2004**, *126*, 14452–14458.
- (13) Ajayaghosh, A.; Praveen, V. K. *Acc. Chem. Res.* **2007**, *40*, 644–656.
- (14) Ghosh, S.; Li, X. Q.; Stepanenko, V.; Wurthner, F. *Chem.—Eur. J.* **2008**, *14*, 11343–11357.
- (15) Hartgerink, J. D.; Zubarev, E. R.; Stupp, S. I. *Curr. Opin. Solid State Mater. Sci.* **2001**, *5*, 355–361.
- (16) Hill, J. P.; Jin, W. S.; Kosaka, A.; Fukushima, T.; Ichihara, H.; Shimomura, T.; Ito, K.; Hashizume, T.; Ishii, N.; Aida, T. *Science* **2004**, *304*, 1481–1483.
- (17) Hoebe, F. J. M.; Jonkheijm, P.; Meijer, E. W.; Schenning, A. P. H. J. *Chem. Rev.* **2005**, *105*, 1491–1546.
- (18) Kaiser, T. E.; Wang, H.; Stepanenko, V.; Wurthner, F. *Angew. Chem., Int. Ed.* **2007**, *46*, 5541–5544.
- (19) Kawano, S.; Fujita, N.; Shinkai, S. *Chem.—Eur. J.* **2005**, *11*, 4735–4742.
- (20) Palmer, L. C.; Stupp, S. I. *Acc. Chem. Res.* **2008**, *41*, 1674–1684.
- (21) Schillinger, E. K.; Mena-Osteritz, E.; Hentschel, J.; Borner, H. G.; Bauerle, P. *Adv. Mater.* **2009**, *21*, 1562–1567.
- (22) Stone, D. A.; Hsu, L.; Stupp, S. I. *Soft Matter* **2009**, *5*, 1990–1993.
- (23) Sugiyasu, K.; Fujita, N.; Shinkai, S. *Angew. Chem., Int. Ed.* **2004**, *43*, 1229–1233.
- (24) Pratihari, P.; Ghosh, S.; Stepanenko, V.; Patwardhan, S.; Grozema, F. C.; Siebbeles, L. D. A.; Wurthner, F. *Beilstein J. Org. Chem.* **2010**, *6*, 1070–1078.
- (25) Coates, I. A.; Smith, D. K. *Chem.—Eur. J.* **2009**, *15*, 6340–6344.
- (26) Wurthner, F.; Bauer, C.; Stepanenko, V.; Yagai, S. *Adv. Mater.* **2005**, *20*, 1695–1698.
- (27) Prasanthkumar, S.; Gopal, A.; Ajayaghosh, A. *J. Am. Chem. Soc.* **2010**, *132*, 13206–13207.
- (28) Prasanthkumar, S.; Saeki, A.; Seki, S.; Ajayaghosh, A. *J. Am. Chem. Soc.* **2010**, *132*, 8866–8867.
- (29) Hulvat, J. F.; Sofos, M.; Tajima, K.; Stupp, S. I. *J. Am. Chem. Soc.* **2005**, *127*, 366–372.
- (30) Tsai, W. W.; Li, L. S.; Cui, H. G.; Jiang, H. Z.; Stupp, S. I. *Tetrahedron* **2008**, *64*, 8504–8514.
- (31) Tsai, W. W.; Tevis, I. D.; Tayi, A. S.; Cui, H.; Stupp, S. I. *J. Phys. Chem. B* **2010**, *114*, 14778–14786.
- (32) Mannsfeld, S. C. B.; Locklin, J.; Reese, C.; Roberts, M. E.; Lovinger, A. J.; Bao, Z. *Adv. Funct. Mater.* **2007**, *17*, 1617–1622.
- (33) Hernandez, V.; Castiglioni, C.; Delzoppo, M.; Zerbi, G. *Phys. Rev. B* **1994**, *50*, 9815–9823.
- (34) Leclere, P.; Surin, M.; Viville, P.; Lazzaroni, R.; Kilbinger, A. F. M.; Henze, O.; Feast, W. J.; Cavallini, M.; Biscarini, F.; Schenning, A.; Meijer, E. W. *Chem. Mater.* **2004**, *16*, 4452–4466.
- (35) Fichou, D. J. *Mater. Chem.* **2000**, *10*, 571–588.
- (36) Tamayo, A. B.; Walker, B.; Nguyen, T. Q. *J. Phys. Chem. C* **2008**, *112*, 11545–11551.
- (37) Tang, W. H.; Hai, J. F.; Dai, Y.; Huang, Z. J.; Lu, B. Q.; Yuan, F.; Tang, J. A.; Zhang, F. J. *Sol. Energy Mater. Sol. Cells* **2010**, *94*, 1963–1979.
- (38) Geng, J. F.; Zhou, W. Z.; Skelton, P.; Yue, W. B.; Kinloch, I. A.; Windle, A. H.; Johnson, B. F. G. *J. Am. Chem. Soc.* **2008**, *130*, 2527–2534.
- (39) Jin, Y. Z.; Curry, R. J.; Sloan, J.; Hatton, R. A.; Chong, L. C.; Blanchard, N.; Stolojan, V.; Kroto, H. W.; Silva, S. R. P. *J. Mater. Chem.* **2006**, *16*, 3715–3720.
- (40) Malik, S.; Fujita, N.; Mukhopadhyay, P.; Goto, Y.; Kaneko, K.; Ikeda, T.; Shinkai, S. *J. Mater. Chem.* **2007**, *17*, 2454–2458.
- (41) Miyazawa, K.; Hamamoto, K.; Nagata, S.; Suga, T. *J. Mater. Res.* **2003**, *18*, 1096–1103.
- (42) Miyazawa, K.; Kuwawaki, Y.; Obayashi, A.; Kuwabara, M. *J. Mater. Res.* **2002**, *17*, 83–88.
- (43) Nakanishi, T. *Chem. Commun.* **2010**, *46*, 3425–3436.
- (44) Nakanishi, T.; Ariga, K.; Michinobu, T.; Yoshida, K.; Takahashi, H.; Teranishi, T.; Mohwald, H.; Kurth, D. G. *Small* **2007**, *3*, 2019–2023.
- (45) Sathish, M.; Miyazawa, K. *J. Am. Chem. Soc.* **2007**, *129*, 13816–13817.
- (46) Sathish, M.; Miyazawa, K.; Hill, J. P.; Ariga, K. *J. Am. Chem. Soc.* **2009**, *131*, 6372–6373.
- (47) Tsuchiya, T.; et al. *J. Am. Chem. Soc.* **2008**, *130*, 450–451.
- (48) Wakahara, T.; Sathish, M.; Miyazawa, K.; Hu, C. P.; Tateyama, Y.; Nemoto, Y.; Sasaki, T.; Ito, O. *J. Am. Chem. Soc.* **2009**, *131*, 9940–9944.

- (49) Wang, L.; Liu, B. B.; Liu, D.; Yao, M. G.; Hou, Y. Y.; Yu, S. D.; Cui, T.; Li, D. M.; Zou, G. T.; Iwasiewicz, A.; Sundqvist, B. *Adv. Mater.* **2006**, *18*, 1883–1888.
- (50) Zhang, Y.; Liu, W.; Jiang, L.; Fan, L. Z.; Wang, C. R.; Hu, W. P.; Zhong, H. Z.; Li, Y. F.; Yang, S. H. *J. Mater. Chem.* **2010**, *20*, 953–956.
- (51) Capito, R. M.; Azevedo, H. S.; Velichko, Y. S.; Mata, A.; Stupp, S. I. *Science* **2008**, *319*, 1812–1816.
- (52) Cha, S. I.; Miyazawa, K.; Kim, J. D. *Chem. Mater.* **2008**, *20*, 1667–1669.
- (53) Cha, S. I.; Miyazawa, K.; Kim, Y. K.; Lee, D. Y.; Kim, J. D. *J. Nanosci. Nanotechnol.* **2011**, *11*, 3374–3380.
- (54) Zaworotko, M. J. *Cryst. Growth Des.* **2007**, *7*, 4–9.
- (55) Yigit, M. V.; Biyikli, K.; Moulton, B.; MacDonald, J. C. *Cryst. Growth Des.* **2006**, *6*, 63–69.
- (56) Moulton, B.; Zaworotko, M. J. *Chem. Rev.* **2001**, *101*, 1629–1658.
- (57) MacDonald, J. C.; Dorrestein, P. C.; Pilley, M. M.; Foote, M. M.; Lundburg, J. L.; Henning, R. W.; Schultz, A. J.; Manson, J. L. *J. Am. Chem. Soc.* **2000**, *122*, 11692–11702.
- (58) Stone, D. A.; Tayi, A. S.; Goldberger, J. E.; Palmer, L. C.; Stupp, S. I. *Chem. Commun.* **2011**, *47*, 5702–5704.
- (59) Messmore, B. W.; Sukerkar, P. A.; Stupp, S. I. *J. Am. Chem. Soc.* **2005**, *127*, 7992–7993.
- (60) Zubarev, E. R.; Pralle, M. U.; Sone, E. D.; Stupp, S. I. *J. Am. Chem. Soc.* **2001**, *123*, 4105–4106.
- (61) Zubarev, E. R.; Sone, E. D.; Stupp, S. I. *Chem.—Eur. J.* **2006**, *12*, 7313–7327.
- (62) Kastler, M.; Pisula, W.; Wasserfallen, D.; Pakula, T.; Mullen, K. *J. Am. Chem. Soc.* **2005**, *127*, 4286–4296.
- (63) Whitten, D. G. *Acc. Chem. Res.* **1993**, *26*, 502–509.
- (64) Ahn, S.; Matzger, A. J. *J. Am. Chem. Soc.* **2010**, *132*, 11364–11371.
- (65) Kim, K.; Plass, K. E.; Matzger, A. J. *Langmuir* **2003**, *19*, 7149–7152.
- (66) Morrison, C. N.; Ahn, S.; Schnobrich, J. K.; Matzger, A. J. *Langmuir* **2011**, *27*, 936–942.
- (67) Edwards, W.; Lagadec, C. A.; Smith, D. K. *Soft Matter* **2011**, *7*, 110–117.
- (68) Jonkheijm, P.; van der Schoot, P.; Schenning, A.; Meijer, E. W. *Science* **2006**, *313*, 80–83.
- (69) Desgranges, C.; Delhommelle, J. *J. Am. Chem. Soc.* **2006**, *128*, 15104–15105.
- (70) Kramer, M.; Hoffman, V. *Opt. Mater.* **1998**, *9*, 65–69.
- (71) Coakley, K. M.; Liu, Y. X.; Goh, C.; McGehee, M. D. *MRS Bull.* **2005**, *30*, 37–40.
- (72) Herman, D. J.; Goldberger, J. E.; Chao, S.; Martin, D. T.; Stupp, S. I. *ACS Nano* **2011**, *5*, 565–573.